Broadband coupling transducers for magneto-inductive cables

2010 J. Phys. D: Appl. Phys. 43 285003

(http://iopscience.iop.org/0022-3727/43/28/285003)

J. Phys. D: Appl. Phys. **43** (2010) 285003 (7pp) doi:10.1088/0022-3727/43/28/285003

Broadband coupling transducers for magneto-inductive cables

R R A Syms[1], **L Solymar and I R Young**

Optical and Semiconductor Devices Group, EEE Department, Imperial College London, Exhibition Road, London SW7 2AZ, UK

E-mail: r.syms@imperial.ac.uk

Received 29 March 2010, in final form 6 June 2010
Published 28 June 2010
Online at stacks.iop.org/JPhysD/43/285003

Abstract
A broadband resonant transducer capable of low-loss coupling between magneto-inductive (MI) waveguides and a real impedance is introduced. The transducer is an L–C circuit resonating at the resonant frequency of the elements forming the guide. However, the values of the components in the transducer are different, and chosen to obtain two separate nulls in reflection so that low reflection is obtained over a wide spectral range. The transducer can be incorporated into the MI waveguide itself, allowing a connection between a MI cable and a conventional system to be made as a simple splice. The design is confirmed using 2 m length of low-loss thin-film MI cables formed using copper-clad polyimide and operating near 100 MHz frequency.

1. Introduction

Magneto-inductive (MI) waveguides are periodic low-frequency electrical structures, formed by magnetically coupling a set of lumped-element L–C circuits [1]. The properties of linear arrangements and 2D and 3D MI arrays have been extensively studied [2–6]. Propagation losses have been reduced [7], and the effects of non-nearest neighbour interactions [8], bi-periodicity [9], coupling to electromagnetic waves [10] and retardation [11] have all been considered. Although the first demonstrations used simple resonant loops, MI waveguides have also been formed as planar structures [12] and thin-film cables [13]. The latter have potential applications as patient-safe cable in magnetic resonance imaging [14, 15]. Many MI devices have been proposed or demonstrated, including magnetic flux concentrators [16], delay lines [12], filters [17], directional couplers [4, 18], splitters [19], lenses for near-field imaging [20–22] and detectors for magnetic resonance imaging [23]. Parametric amplification has been considered as a method of reducing propagation losses [24, 25].

Despite this effort, losses per metre have historically been high (150 dB m^{-1} in [1] and 50 dB m^{-1} in [7]), propagation distances have been limited, and end-reflections have mainly been ignored. However, the demonstration of losses of ≈2.5 dB m^{-1} in thin-film cables [13] has re-affirmed the need for an effective transducer for coupling to a conventional transmission line or for termination. Without such a transducer, it will be difficult to construct any high-performance MI system. Although multi-element absorbers have been proposed [26], these do not solve the coupling problem. In this paper, we consider possibilities for inductive coupling to a MI waveguide, and demonstrate a simple broadband transducer that can be constructed from passive components. The theory of matching is described in section 2, transducer optimization is explored in more detail in section 3, experimental verification is presented in section 4 and conclusions are drawn in section 5.

2. Matching to MI waveguides

We first consider the principle of matching a MI waveguide to a real load. Figure 1(a) shows the equivalent circuit of an ideal, loss-less guide, formed from a set of L–C resonators coupled to their nearest neighbours by a mutual inductance M. Away from any termination ($n < 0$) the equation governing the current I_n in the nth element at angular frequency ω can be found from Kirchhoff's voltage law as [1]

$$\{\mathrm{j}\omega L + 1/\mathrm{j}\omega C\}I_n + \mathrm{j}\omega M\{I_{n-1} + I_{n+1}\} = 0. \qquad (1)$$

A solution can be found by assuming that I_n is the travelling wave $I_n = I_0 \exp(\pm \mathrm{j}nka)$, where I_0 is the wave amplitude,

[1] Author to whom any correspondence should be addressed.

ka is the phase shift per element, k is the propagation constant and a is the period. Substitution into equation (1) yields the well-known dispersion equation:

$$(1 - \omega_0^2/\omega^2) + \kappa \cos(ka) = 0. \tag{2}$$

Here $\omega_0^2 = 1/LC$ is the angular resonant frequency and $\kappa = 2M/L$ the coupling coefficient. For positive κ, propagation can only take place for ω/ω_0 between $1/\sqrt{(1+\kappa)}$ and $1/\sqrt{(1-\kappa)}$. The effect of loss may be modelled by repeating the analysis, assuming the presence of a resistor R in each resonant loop [1]. If this is done, the dispersion equation is modified to $(1 - \omega_0^2/\omega^2 - \mathrm{j}/Q) + \kappa \cos(ka) = 0$, where $Q = \omega L/R$ is the Q-factor. Assuming a complex-valued propagation constant $ka = k'a - \mathrm{j}k''a$, and further assuming that $k''a$ is small, it can be shown that $k''a = 1/\{\kappa Q \sin(k'a)\}$. Losses are lowest at mid-band, and strong coupling and a high Q-factor are required for low loss.

In [2], it was shown that a non-reflective termination is formed by inserting an impedance Z_0 into the last (0th) element of the waveguide, where Z_0 is given by

$$Z_0 = \mathrm{j}\omega M \exp(-\mathrm{j}ka). \tag{3}$$

At mid-band, when $\omega = \omega_0$ and $ka = \pi/2$, Z_0 reduces to the real value $Z_{0\mathrm{M}} = \omega_0 M$. Thus, in principle it should be possible to couple a MI waveguide to a conventional transmission line (which has real impedance) if M is appropriately chosen. Unfortunately, Z_0 is complex away from the band centre, and moreover as expressed here is a function of both ka and ω. Consequently, equation (3) has so far represented a mathematical contrivance, rather than an element that can be realized. Further development of MI systems clearly requires simple circuits that can approximate this impedance.

In a search for suitable circuits we consider the termination in figure 1(*b*). Here the final element of a MI waveguide is coupled via a mutual inductance M' to a loop containing an inductance L', a capacitance C' and a real load R_L, which will typically represent a 50 Ω system. The loop is resonant at an angular frequency $\omega_0' = 1/L'C'$, but may be considered non-resonant when ω_0' is zero. For the final elements, the circuit equations are

$$\begin{aligned} \{\mathrm{j}\omega L + 1/\mathrm{j}\omega C\} I_0 + \mathrm{j}\omega M I_{-1} + \mathrm{j}\omega M' I_\mathrm{L} &= 0, \\ \{R_\mathrm{L} + \mathrm{j}(\omega L' - 1/\omega C')\} I_\mathrm{L} + \mathrm{j}\omega M' I_0 &= 0. \end{aligned} \tag{4}$$

Combining equations (4), we obtain for the 0th element:

$$\{\mathrm{j}\omega L + 1/\mathrm{j}\omega C + Z_\mathrm{L}\} I_0 + \mathrm{j}\omega M I_{-1} = 0. \tag{5}$$

Here Z_L is a load that has effectively been inserted into the 0th element, given by

$$Z_\mathrm{L} = \omega^2 M'^2 / \{R_\mathrm{L} + \mathrm{j}\omega L'(1 - \omega_0'^2/\omega^2)\}. \tag{6}$$

We may evaluate the performance of Z_L as a termination by considering the reflection of current waves as shown in figure 1(*c*). Assuming solutions of equations (1) and (5) as the sum of incident and reflected waves, i.e. as $I_\mathrm{n} = I_\mathrm{I} \exp(-\mathrm{j}nka) + I_\mathrm{R} \exp(+\mathrm{j}ka)$, substituting into equation (5)

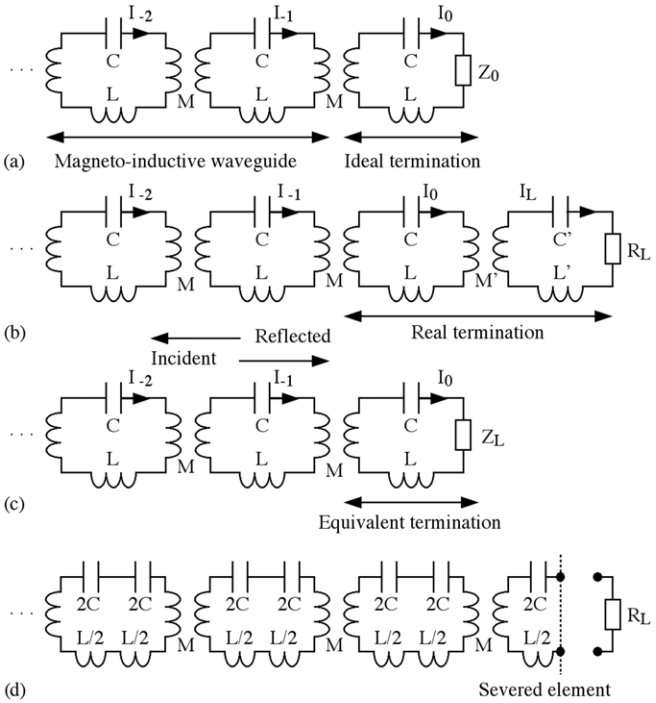

Figure 1. MI waveguide, with (*a*) ideal termination, (*b*) real termination, (*c*) equivalent termination and (*d*) self-termination.

and using equation (2) we can obtain the reflection coefficient $\Gamma = I_\mathrm{R}/I_\mathrm{I}$ as

$$\Gamma = -\{Z_\mathrm{L} - Z_0\}/\{Z_\mathrm{L} + Z_0^*\} \tag{7}$$

Equation (7) is similar to the reflection coefficient for current waves obtained when a conventional transmission line is terminated with a load. However, due to the presence of a complex conjugate term, it is clearly not identical.

Since the current in element zero, which passes through the effective load, is $I_0 = I_\mathrm{I} + I_\mathrm{R}$, we can also define a transmission coefficient as $T = I_0/I_\mathrm{I} = (1 + \Gamma)$, or

$$T = 2\mathrm{Re}(Z_0)/\{Z_\mathrm{L} + Z_0^*\}. \tag{8}$$

Equation (8) is again similar, but not identical to the conventional transmission coefficient, due to the presence of a real operator. It is simple to show that Γ and T satisfy the power conservation relation:

$$\Gamma\Gamma^* + TT^* \mathrm{Re}(Z_\mathrm{L})/\mathrm{Re}(Z_0) = 1 \tag{9}$$

Once again, equation (9) is similar to the corresponding result for real-valued systems.

Different terminations can be compared by plotting the scattering parameter S_{11} in dB, as

$$S_{11} \approx 10 \log_{10}\{|\Gamma|^2\}. \tag{10}$$

Equation (7) implies that Z_L should be chosen to approximate Z_0 as far as possible. We now compare a number of possibilities, assuming for simplicity that $Z_{0\mathrm{M}} = R_\mathrm{L}$ and that $M' = M$.

Figure 2 shows the frequency variation of S_{11} obtained in a non-resonant transducer for different values of L'/L,

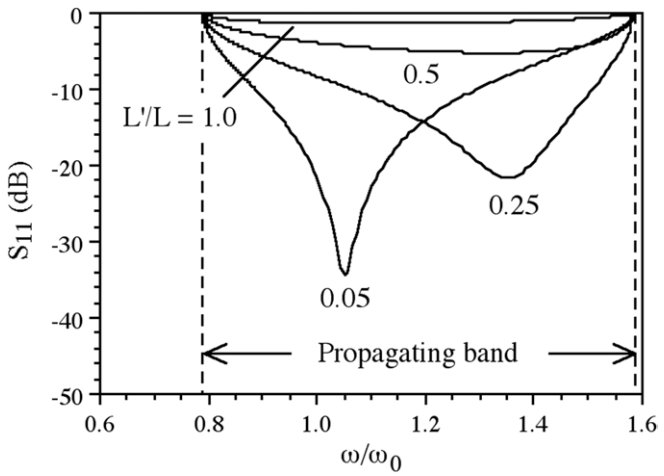

Figure 2. Frequency variation of the scattering parameter S_{11} for non-resonant transducers calculated assuming $M' = M$, $\kappa = 0.6$ and different values of L'/L.

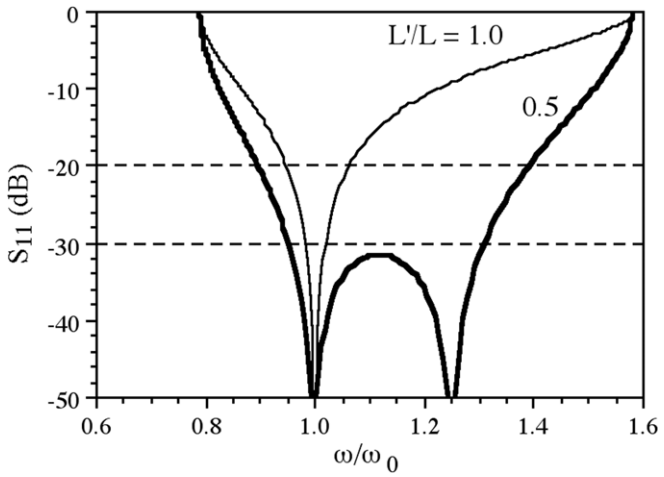

Figure 3. Frequency variation of the scattering parameter S_{11} for resonant transducers, calculated assuming $M' = M$, $\kappa = 0.6$, $\omega_0' = \omega_0$ and different values of L'/L.

calculated assuming the typical coupling coefficient $\kappa = 0.6$. Propagation can take place over the band $0.79 \leqslant \omega/\omega_0 \leqslant 1.58$, and S_{11} rises to 0 dB at the band edges. Within the band, S_{11} reduces somewhat. However, when $L'/L = 1$, the reflection coefficient is generally high and the transducer is correspondingly ineffective. As L'/L reduces, a deeper and deeper minimum in S_{11} develops, and gradually shifts towards $\omega/\omega_0 = 1$. These results imply that the performance of the transducer improves as L'/L reduces, and that the best result is obtained when only a small reactance is inserted into the final loop. However, the best that can be achieved still only represents a narrow-band impedance match. Furthermore, the minimum in S_{11} is relatively high (−35 dB), and even this result is only obtained for very small values of L'/L, when it may be difficult to maintain $M'/M = 1$.

The inserted reactance can clearly be cancelled more effectively if the transducer is made resonant. Figure 3 shows the corresponding variation of S_{11} obtained for a resonant transducer, calculated assuming that $\kappa = 0.6$ and that L' and C' are chosen so that $\omega_0' = \omega_0$. Results are again shown for different values of L'/L. The most obvious choice of $L'/L = 1$ provides a complete null in reflectivity when $\omega/\omega_0 = 1$. However, this result again only represents a narrow-band match. In contrast, the less obvious choice of $L'/L = 0.5$ provides two nulls in reflectivity, the first again being at $\omega/\omega_0 = 1$. Because the nulls are widely separated, low reflectivity is obtained over a wide band. For example, S_{11} is less than −20 dB for 65% of the pass-band, and less than −30 dB for 45%. This form of transducer is extremely effective. Importantly, it can be realized very conveniently as shown in figure 1(*d*). Here each resonant element in a MI waveguide is now formed from two separate inductors of value $L/2$, and two capacitors of value 2C. If half the final element is simply removed, the remainder may then be connected directly to a resistive load. This modification allows MI waveguides of arbitrary length to be terminated without the need for additional components. To realize such an arrangement, all that is required is to stagger the inductors and capacitors in each unit cell, so that the cell may be exactly bisected using a transverse cut.

3. Transducer optimization

We now consider the broadband resonant transducer in more detail. To understand how it achieves its effect, we introduce the normalized characteristic impedance $Z_{0N} = Z_0/\omega_0 M$, obtained from equation (3) as

$$Z_{0N} = w/\{\sin(ka) - \mathrm{j}\cos(ka)\}. \tag{11}$$

Here $w = \omega/\omega_0$ is a normalized frequency. Using the dispersion equation (2), Z_{0N} may be written alternatively as

$$Z_{0N} = w/\{\sqrt{[1-(1-1/w^2)^2/\kappa^2]} + \mathrm{j}(1-1/w^2)/\kappa\}. \tag{12}$$

In this form, Z_{0N} is clearly a function only of w. Consequently it may be compared directly with the corresponding normalized load impedance $Z_{LN}/\omega_0 M$, which may be written as

$$Z_{LN} = w/\{\rho/w\mu^2 + \mathrm{j}(2\lambda/\kappa\mu^2)(1-\eta^2/w^2)\}. \tag{13}$$

Here we have introduced four normalized variables. The first, $\rho = R_L/\omega_0 M$, is the ratio of the R_L to the mid-band impedance of the MI waveguide. The second, $\lambda = L'/L$, is the ratio of the self-inductances in the transducer and the guide, the third, $\mu = M'/M$, is the ratio of mutual inductances and the fourth, $\eta = \omega_0'/\omega_0$, is the ratio of resonant frequencies.

Clearly, reflectivity will be low if the real and imaginary parts of Z_{0N} and Z_{LN} are similar or alternatively if the real and imaginary parts of the normalized admittances $Y_{0N} = 1/Z_{0N}$ and $Y_{LN} = 1/Z_{LN}$ correspond. Considering first the imaginary parts, $\mathrm{Im}(Y_{0N})$ can be made equal to $\mathrm{Im}(Y_{LN})$ for all ω if $\eta = 1$ and $\lambda = \mu^2/2$. If $\mu = 1$, as previously assumed, a complete match in admittance can therefore be obtained if the transducer is resonant at ω_0 and the inductance L' of the transducer is half that of the resonant elements forming the guide.

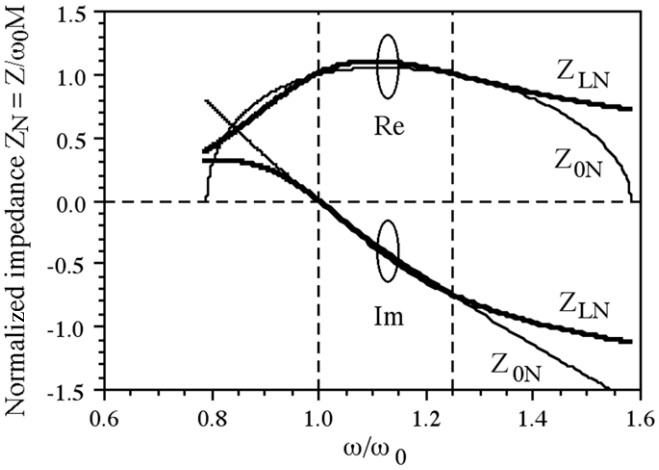

Figure 4. Frequency variation of the real and imaginary parts of the normalized impedance $Z_{0N} = Z_0/\omega_0 M$ (thin lines) and $Z_{LN} = Z_L/\omega_0 M$ (thick lines), calculated assuming $M' = M$, $\kappa = 0.6$, $\omega_0' = \omega_0$ and $L' = L/2$.

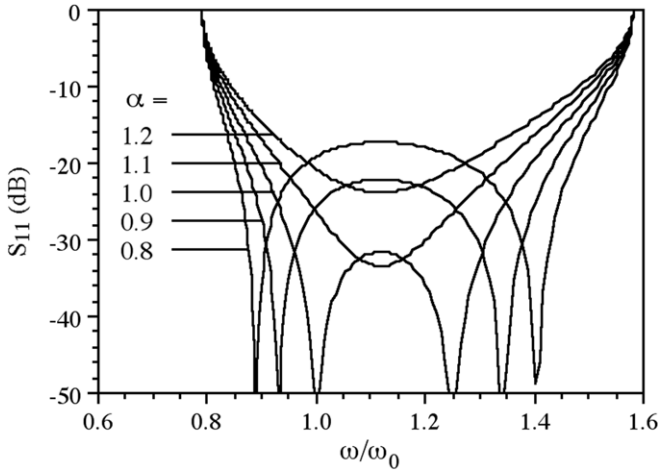

Figure 5. Frequency variation of the scattering parameter S_{11} for resonant transducers, calculated assuming $M' = M$, $\kappa = 0.6$, $L'/L = 0.5$ and different values of α.

Considering now the real parts, and assuming that the transducer is correctly resonant, $\mathrm{Re}(Y_{0N})$ can be made equal to $\mathrm{Re}(Y_{LN})$ if

$$\rho/w\mu^2 = \sqrt{[1-(1-1/w^2)^2/\kappa^2]} \tag{14}$$

Equation (14) is actually a quadratic equation, which can be expanded as

$$w^4\{\kappa^2 - 1\} + w^2\{2 - \alpha^2\kappa^2\} - 1 = 0. \tag{15}$$

Here, $\alpha = \rho/\mu^2$. When $\alpha = 1$, a condition that can be achieved by taking $M' = M$ and $\omega_0 M = R_L$, equation (15) has the simple solutions of $w = 1$ and $w = 1/\sqrt{(1-\kappa^2)}$. Both lie in the propagating band. These results imply that if $\omega_0 M = R_L$, and if the transducer is made resonant at ω_0 using an inductance $L' = L/2$ (which requires a capacitance $C' = 2C$), the imaginary parts of Y_L and Y_0 can be made equal across the band and the real parts at two discrete frequencies. Consequently, Z_0 and Z_L can be equalized at the same two frequencies, and at these points there can be no reflection. These results are confirmed in figure 4, which shows the frequency variations of the real and imaginary parts of Z_{0N} and Z_{LN}, calculated assuming $\kappa = 0.6$. Matching is achieved when $w = \omega/\omega_0 = 1$ and $\omega/\omega_0 = 1/\sqrt{(1-0.6^2)} = 1.25$, the points at which nulls in reflectivity are seen in figure 3. Broadband operation then follows from the existence of these two separate nulls.

A broadband transducer can still be constructed if $\alpha \neq 1$ (for example, if $M' = M$ but $\omega_0 M \neq R_L$). Figure 5 shows the frequency variation of the scattering parameter S_{11} for resonant transducers, calculated assuming $\kappa = 0.6$, and $L'/L = 0.5$ and assuming different values of α. For $\alpha < 1$, there are again two nulls in reflectivity, which move further apart as α reduces. For $\alpha > 1$, there is only a single minimum, not a null. However, in each of the cases shown, the return is generally low over a wide spectral range. These results suggest that the broadband resonant transducer will give reasonable performance even when the mid-band impedance of the MI waveguide is slightly mismatched from R_L.

Finally, it is simple to show that the two nulls in reflectivity just merge together when the roots of equation (15) are repeated. This occurs when

$$(2 - \alpha^2\kappa^2)^2 = 4(1 - \kappa^2) \tag{16}$$

Or when

$$\alpha^4\kappa^2 - 4\alpha^2 + 4 = 0 \tag{17}$$

Equation (17) has the solutions $\alpha = (\sqrt{2}/\kappa)\times\{1 \pm \sqrt{(1-\kappa^2)}\}^{1/2}$. For $\kappa = 0.6$, for example, the solutions are $\alpha = 3.162$ and $\alpha = 1.054$. The latter value is midway between $\alpha = 1$ and $\alpha = 1.1$, and generates a variation in reflectivity with a single null.

4. Experimental verification

Experimental confirmation of the theory of the previous section was provided using thin-film MI cables formed by double-sided patterning of copper-clad polyimide, as described in [13]. Figure 6(*a*) shows the physical arrangement and key dimensions, and figure 6(*b*) a short section of cable. Each resonant element is formed from two inductors and two capacitors. The inductors are single-turn loops of inductance $L/2$, located on either side of a thin substrate, while the capacitors are parallel-plate components of capacitance 2C, which use the substrate as a dielectric interlayer. This arrangement approximates that of figure 1(*d*), although it does not allow a resonant termination to be formed by cutting the cable. Instead, it provides non-resonant terminations of inductance $L' = L/2$, which may be made resonant with additional capacitors. Since the mutual inductances M and M' are the same, this arrangement has normalized parameter values $\lambda = 0.5$ and $\mu = 1$.

Cables were fabricated in 2 m length by the UK company Clarydon (Willenhall, West Midlands). The base material consisted of 25 μm thick Kapton® carrying a 35 μm thick

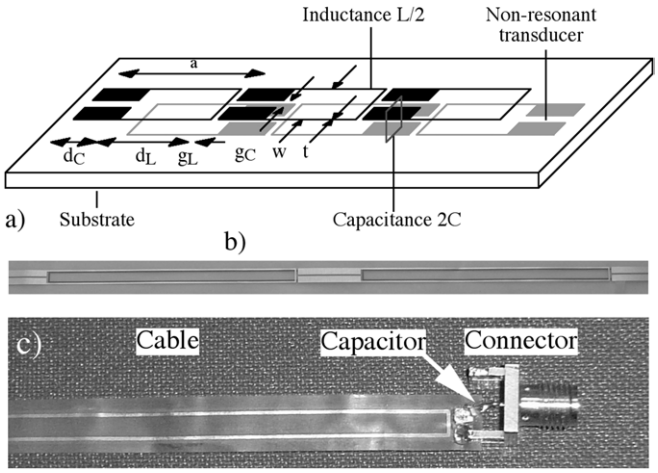

Figure 6. (*a*) Arrangement and (*b*) experimental realization of thin-film MI cable; (*c*) arrangement for resonant connection to conventional co-axial cable.

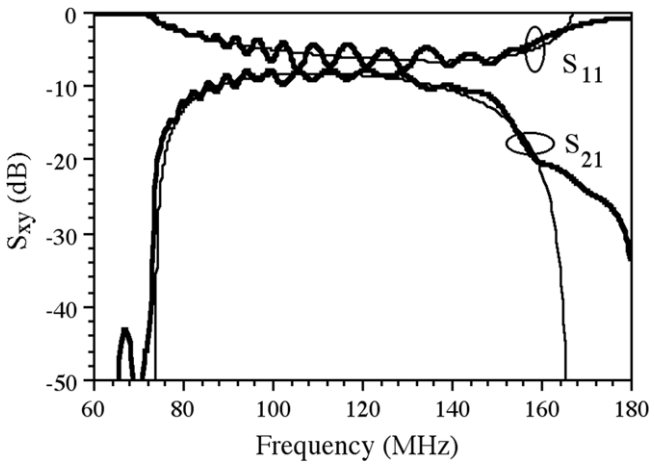

Figure 7. Frequency variation of S_{11} and S_{21} for thin-film MI cable, with non-resonant transducers. Thick lines are experimental data and thin lines are theory.

layer of copper on either side. The copper was patterned by step-and-repeat lithographic exposure to a pair of 1 m long photomasks, followed by wet etching. The photomasks contained a set of MI waveguides with different parameters. The overall width and length were taken as $w = 4.7$ mm and $a = 100$ mm throughout, so that a 2 m length contained 19 resonant elements. The track width t, and the small gaps g_C and g_L between capacitor plates and between plates and tracks were all taken as 0.5 mm. The main variables were the capacitor and inductor lengths d_C and d_L, which were varied to obtain different properties. Of particular importance were the inductance L, the capacitance C, the mutual inductance M and the Q-factor of the resonant elements. These parameters determine the resonant frequency $f_0 = \omega_0/2\pi$, the coupling coefficient $\kappa = 2M/L$, the mid-band impedance $Z_{0M} = \omega_0 M$ and an imaginary part of the propagation constant.

Electrical performance was evaluated using an Agilent E5061A Electronic Network Analyser (ENA). The inductance was determined by making the transducers resonant at low frequency with a known capacitor and measuring the resonant frequency with a weak inductive probe. The remaining parameters were estimated by attaching SMA-type end-launch connectors as shown in figure 6(*c*), measuring transmission and reflection data, and fitting the data to a theoretical model. Recently, it has been shown that flexible MI cable is very tolerant to bends, due to the extreme stability of the mutual inductance between adjacent elements [27]. Despite this, small reflections tend to mask the appearance of predicted nulls in S_{11}. The smallest overall reflections were therefore obtained with the MI waveguide held straight, using an additional co-axial cable to return the transmitted signal to the ENA.

The theoretical model includes propagation loss but ignores multiple reflections. In this case, the scattering parameters S_{11} and S_{21} for an N-element MI waveguide connected to a source with real output impedance R_L and a similar load are given approximately by

$$S_{11} \approx 10\log_{10}\{|\Gamma|^2\}, \tag{18}$$

$$S_{21} \approx 10\log_{10}\{(1-|\Gamma|^2)\exp(-2Nk''a)(1-|\Gamma|^2)\}. \tag{19}$$

Figure 7 shows a comparison between experimental measurement of the frequency variations of S_{11} and S_{21} and the theory above, for a cable with $d_C = 10$ mm and $d_L \approx 90$ mm. The experimental data show band-limited propagation between 70 MHz and 160 MHz. Overall transmission is high, and S_{21} peaks at -8 dB near 110 MHz. Oscillations in transmission and reflection are due to multiple reflections, and suggest low propagation loss. However, the return is high, and the minimum value of S_{11} is only ≈ -7 dB. These results confirm the poor performance of non-resonant transducers. The agreement between theory and experiment is clearly good, apart from the inability of the simple theory used here to model multiple reflections and a small discrepancy in S_{21} at high frequency.

The combination of direct measurement and matching to theory allowed deduction of the following parameter values. The inductance was estimated as $L = 241$ nH, the resonant frequency as $f_0 = 95$ MHz, the capacitance as $C = 11.6$ pF, the coupling coefficient as $\kappa = 0.675$, the mid-band impedance as $Z_{0M} = 48.6\,\Omega$ and the Q-factor as $Q = 48$ (which in turn implies a mid-band propagation loss of 0.27 dB m^{-1}). The mid-band impedance is clearly close to 50 Ω, and gives a value of $\rho = R_L/Z_0 M = 1.028$.

The terminations were made resonant using surface mount capacitors, using the optimum capacitance value of $2 \times 11.6 \approx 23$ pF. Electrical performance was then re-measured to give the results shown in figure 8. Here, peak transmission has now increased to -5.2 dB, and the oscillations due to multiple reflections have largely disappeared. The return has significantly reduced, and S_{11} is below -25 dB for much of the band. The data are again compared with theory, this time assuming a resonant termination, and good agreement is again obtained. However, the predicted nulls in reflection cannot be seen in the experiment, presumably due to other small reflections from connections. These results confirm the improvement in performance offered by the optimum resonant termination.

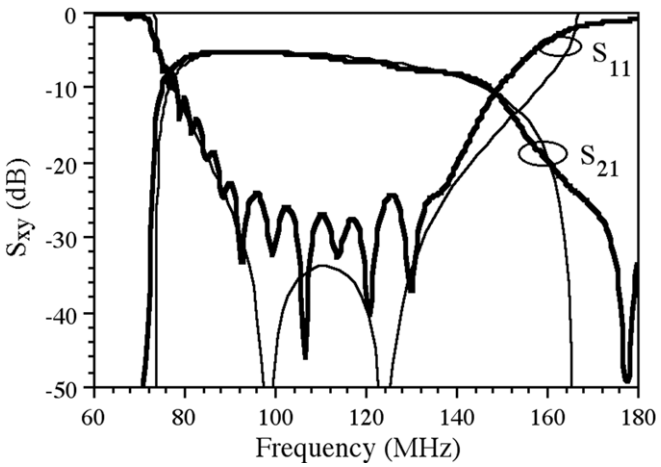

Figure 8. Frequency variation of S_{11} and S_{21} for thin-film MI cable, with resonant transducers. Thick lines are experimental data and thin lines are theory.

5. Conclusions

A simple inductive transducer for coupling a MI waveguide to a real load has been introduced. A theory of reflection from lumped-element coupling transducers has been developed. It has been shown that zero reflection can be obtained at a single frequency if the (real-valued) mid-band impedance of the MI waveguide matches the load, and if the transducer is resonant at the same frequency as the resonant elements forming the guide. If in addition the inductance of the transducer is half that used in the resonant elements and the capacitance is correspondingly double, matching to the load can also be achieved at a second frequency. Since zero reflection is now obtained at two separate frequencies, low reflectivity can be obtained over a broad spectral range. The theory has been compared with experimental results obtained from thin-film MI cable. Excellent agreement has been obtained, and the improvement in performance offered by the optimized resonant transducer has been confirmed by comparison with a non-resonant equivalent.

Other more complicated transducer designs can doubtless be developed to achieve improved broadband performance. However, the simple design presented here has the important advantage that a transducer with exactly the required properties can be obtained from the waveguide itself, if the resonant elements are formed using pairs of inductors and capacitors in series, rather than single components. As a result, a connection between a MI waveguide and a system with real impedance may be obtained simply by splicing, exactly as is done for other cable types such as co-axial cable. The demonstration of a simple arrangement for coupling should significantly increase potential applications for MI waveguides.

References

[1] Shamonina E, Kalinin V A, Ringhofer K H and Solymar L 2002 Magneto-inductive waveguide *Electron. Lett.* **38** 371–3

[2] Shamonina E, Kalinin V A, Ringhofer K H and Solymar L 2002 Magnetoinductive waves in one, two and three dimensions *J. Appl. Phys.* **92** 6252–61

[3] Wiltshire M C K, Shamonina E, Young I R and Solymar L 2003 Dispersion characteristics of magneto-inductive waves: comparison between theory and experiment *Electron. Lett.* **39** 215–7

[4] Shamonina E and Solymar L 2004 Magneto-inductive waves supported by metamaterial elements: components for a one-dimensional waveguide *J. Phys. D. Appl. Phys.* **37** 362–7

[5] Maslovski S, Ikonen P, Kolmakov I and Tretyakov S 2005 Artificial magnetic materials based on the new magnetic particle: metasolenoid *Prog. electromagn. Res.* **54** 61–81

[6] Jylhä L, Maslovski S and Tretyakov 2009 Traveling waves along the metasolenoid *Progress in Electromagnetics Research Symp. (Cambridge, MA, 26–29 March 2009)*

[7] Syms R R A, Young I R and Solymar L 2006 Low loss magneto-inductive waveguides *J. Phys. D. Appl. Phys.* **39** 3945–51

[8] Syms R R A, Sydoruk O, Shamonina E and Solymar L 2007 Higher order interactions in magneto-inductive waveguides *Metamaterials* **1** 44–51

[9] Radkovskaya A, Sydoruk O, Shamonin M, Shamonina E, Stevens C J, Faulkner G, Edwards D J and Solymar L 2007 Experimental study of a bi-periodic magnetoinductive waveguide: comparison with theory *IET Microw. Antennas Propag.* **1** 80–3

[10] Syms R R A, Shamonina E, Kalinin V and Solymar L 2005 A theory of metamaterials based on periodically loaded transmission lines: interaction between magneto-inductive and electro-magnetic waves *J. Appl. Phys.* **97** 064909

[11] Radkovskaya A, Shamonin M, Stevens C J, Faulkner G, Edwards D J, Shamonina E and Solymar L 2006 An experimental study of the properties of magnetoinductive waves in the presence of retardation *J. Magn. Magn. Mater.* **300** 29–32

[12] Freire M J, Marques R, Medina F, Laso M A G and Martin F 2004 Planar magneto-inductive wave transducers: theory and applications *Appl. Phys. Lett.* **85** 4439–41

[13] Syms R R A, Solymar L, Young I R and Floume T Thin-film magneto-inductive cable *J. Phys. D. Appl. Phys.* submitted

[14] Syms R R A, Solymar L and Young I R 2010 Periodic analysis of MR-safe transmission lines *IEEE J. Sel. Top. Quantum Electron* **16** 433–40

[15] Weiss S, Vernickel P, Schaeffter T, Schulz V and Gleich B 2005 Transmission line for improved RF safety of interventional devices *Mag. Res. Med.* **54** 182–9

[16] Wiltshire M C K, Shamonina E, Young I R and Solymar L 2003 Resonant magnetic concentrators *Progress in Electromagnetics Research Symp. PIERS 2003 (Honolulu, HI,13–16 October)*

[17] Nefedov I S and Tretyakov S A 2005 On potential applications of metamaterials for the design of broadband phase shifters *Microw. Opt. Technol. Lett.* **145** 98–102

[18] Radkovskaya A, Sydoruk O, Shamonin M, Stevens C J, Faulkner G, Edwards D J, Shamonina E and Solymar L 2007 Transmission properties of two shifted magnetoinductive waveguides *Microw. Opt. Technol. Lett.* **49** 1054–8

[19] Syms R R A, Shamonina A and Solymar L 2006 Magneto-inductive waveguide devices *IEE Proc. Microw. Antennas Propag.* **153** 111–21

[20] Freire M J and Marques R 2005 Planar magnetoinductive lens for three-dimensional subwavelength imaging *Appl. Phys. Lett.* **86** 182505

[21] Sydoruk O, Shamonin M, Radkovskaya A, Zhuromskyy O, Shamonona E, Trautner R, Stevens C J, Faulkner G, Edwards D J and Solymar L 2007 Mechanism of

subwavelength imaging with bilayered magnetic metamaterials: theory and experiment *J. Appl. Phys.* **101** 073903

[22] Freire M J, Marques R and Jelinek L 2008 Experimental demonstration of a $\mu = -1$ metamaterial lens for magnetic resonance imaging *Appl. Phys. Lett.* **93** 231108

[23] Solymar L, Zhuromskyy O, Sydoruk O, Shamonina E, Young I R and Syms R R A 2006 Rotational resonance of magnetoinductive waves: basic concept and application to nuclear magnetic resonance *J. Appl. Phys.* **99** 123908

[24] Sydoruk O, Shamonina E and Solymar L 2007 Parametric amplification in coupled magnetoinductive waveguides *J. Phys. D: Appl. Phys.* **40** 6879–87

[25] Syms R R A, Young I R and Solymar L 2008 Three-frequency parametric amplification in magneto-inductive ring resonators *Metamaterials* **2** 122–34

[26] Syms R R A, Solymar L and Shamonina E 2005 Absorbing terminations for magneto-inductive waveguides *IEE Proc. Microw. Antennas Propag.* **152** 77–81

[27] Syms R R A and Solymar L Bends in magneto-inductive waveguides *Metamaterials* at press